ARTICLE NO. 78-1186R

A80-034

Turbulent Radiating Shock Layers with Coupled Ablation Injection

20003
20012
90005

James N. Moss* and Ann L. Simmonds†
NASA Langley Research Center, Hampton, Va.
and
E. Clay Anderson‡
DCW Industries, Inc., Studio City, Calif.

This paper provides a description of the potential impact of turbulence on a radiating flowfield with large surface blowing. This is accomplished by calculating the forebody flowfield with coupled carbon-phenolic mass injection for a probe entering the Jupiter atmosphere. Both laminar and turbulent flow conditions are assumed. For the no-blowing solutions, turbulence is shown to have no impact on the surface radiative heating; however, with ablation injection, turbulence significantly increases the surface radiative heating rate. This occurs because turbulence promotes mixing of the high-temperature gases in the outer region of the shock layer with the ablation products, thus thinning the cool molecular gases near the surface, which are responsible for blocking much of the radiation.

Nomenclature

C_D = drag coefficient
C_i = mass fraction of species $i = \rho_i/\rho$
$\tilde{C}_l$ = mass fraction of element l
C_p = frozen specific heat of mixture $= \sum_{i=1}^{N} C_i C_{p,i}$
$C_{p,i}$ = specific heat of species $i = C^*_{p,i}/C^*_{p,\infty}$
D_{ij} = binary diffusion coefficients
H = $h + (u^2/2)$
h = enthalpy of mixture $= \sum_{i=1}^{N} C_i h_i$
h_i = enthalpy of species $i = h^*_i/U^{*2}_\infty$
j = flow index (0 for plane, 1 for axisymmetric)
K = thermal conductivity of mixture $= K^*/\mu_{\text{ref}} C^*_{p,\infty}$
M^* = molecular weight
$\bar{M}^*$ = molecular weight of mixture
$\dot{m}$ = mass injection rate $= \dot{m}^*/\rho^*_\infty U^*_\infty$
N = number of species
N_{Le} = Lewis number $= \rho^* D^*_{ij} C^*_p/K^*$
$N_{Le,T}$ = turbulent Lewis number
N_{Pr} = Prandtl number $= \mu^* C^*_p/K^*$
$N_{Pr,T}$ = turbulent Prandtl number $= \mu^*_T C^*_p/K^*_T$
N_{Re} = Reynolds number $= \rho^*_\infty U^*_\infty r^*_n/\mu^*_\infty$
N_{Sc} = Schmidt number $= N_{Pr}/N_{Le}$
n = coordinate measured normal to body $= n^*/R^*_N$
p = pressure $= p^*/[\rho^*_\infty (U^*_\infty)^2]$
Q = divergence of net radiant heat flux $= Q^* R^*_N/\rho^*_\infty U^{*3}_\infty$
q_r = net radiant heat flux in n direction $= q^*_r/\rho^*_\infty U^{*3}_\infty$
$q_r^{(-)}$ = component of radiant flux toward the wall
$-q_{c,w}$ = convective heat flux to the wall [Eq. (7)]
R^* = universal gas constant
R^*_N = nose radius
r = radius measured from axis of symmetry to point on body surface $= r^*/R^*_N$
s = coordinate measured along body surface $= s^*/R^*_N$
T = temperature $= T^*/T^*_{\text{ref}}$
T^*_{ref} = temperature $= (U^*_\infty)^2/C^*_{p,\infty}$
U^*_∞ = freestream velocity
u = velocity component tangent to body surface $= u^*/U^*_\infty$
v = velocity component normal to body surface $= v^*/U^*_\infty$
α = shock angle defined in Fig. 1
δ_{il} = number of atoms of the lth element in species i
ϵ^+ = normalized eddy viscosity $= \mu_T/\mu$
θ = body angle defined in Fig. 1
κ = body curvature
μ = molecular viscosity $= \mu^*/\mu^*(T^*_{\text{ref}})$
μ_T = eddy viscosity $= \mu^*_T/\mu^*(T^*_{\text{ref}})$
ξ = coordinate measured along body surface $= s$
ρ = density of mixture $= \rho^*/\rho^*_\infty$
σ = Reynolds number parameter $= [\mu^*(T^*_{\text{ref}})/\rho^*_\infty U^*_\infty R^*_N]^{1/2}$
σ^* = Stefan-Boltzmann constant
$\phi_{1,2,3}$ = quantities defined by Eqs. (4b, 4c, and 4d)

Superscripts

j = 0 for plane flow, 1 for axisymmetric flow
$*$ = dimensional quantity

Subscripts

i = ith species
l = lth element
s = shock
w = wall
∞ = freestream
ν = radiation frequency

Presented as Paper 78-1186 at the 11th Fluid and Plasma Dynamics Conference, Seattle, Wash., July 10-12, 1978; submitted June 4, 1979; revision received Nov. 2, 1979. This paper is declared a work of the U.S. Government and therefore is in the public domain. Reprints of this article may be ordered from AIAA Special Publications, 1290 Avenue of the Americas, New York, N.Y. 10019. Order by Article No. at top of page. Member price $2.00 each, nonmember, $3.00 each. **Remittance must accompany order.**

Index categories: Radiatively Coupled Flows and Heat Transfer; Boundary Layers and Convective Heat Transfer—Turbulent; Radiation and Radiative Heat Transfer.

*Research Engineer, Aerothermodynamics Branch, Space Systems Division. Member AIAA.

†Mathematician, Aerothermodynamics Branch, Space Systems Division.

‡Consulting Engineer; currently, Research Engineer, Theoretical Aerodynamics Branch, Subsonic Transonic Aerodynamics Division, NASA Langley Research Center.

Introduction

THE Galileo spacecraft, formerly referred to as the Jupiter orbiter-probe spacecraft, is tentatively scheduled to be launched in January 1982. After more than a 1000-day journey to Jupiter, the probe and orbiter will separate and the Galileo probe will enter Jupiter's atmosphere with an array of scientific instruments. After the fore and aft heat shields are discarded, the instruments will make atmospheric measurements as the probe descends through the pressure-altitude region of 0.1-10 atm. Results obtained from these measurements will provide information concerning the nature and composition of the atmosphere, the location and structure of the clouds, the nature and extent of cloud particles, and the local radiative energy balance.

In order for the Galileo probe to accomplish its scientific objectives, it must first survive the severe aerothermal conditions encountered during entry. The probe's relative entry velocity is 48 km/s. For such an entry velocity, the shock-layer gases that surround the probe forebody will be compressed to temperatures of 10,000-20,000 K, and the surface heating will be due primarily to radiative heating. The intense radiation from the high-temperature gases consists of both continuum and line radiation and leads to mass ablation from the probe surface. Designing a heat shield to withstand the intense heating is a demanding requirement. In fact, the heating is so severe that about 50% of the probe weight will be in the heat shield.

Unfortunately, the aerothermal environment that will be encountered by the Galileo probe cannot be duplicated in any existing ground experimental facilities. Consequently, the design of a heat shield for the Galileo probe must rely extensively on analytical predictions. A number of recent analytical studies (for example, Refs. 1-4) have attempted to improve on the definition of the aerothermal environment that will be encountered by the Galileo probe. A basic unresolved question concerning Jupiter entry heating is the extent to which the high-intensity radiation of the shock layer penetrates the relatively cool gas of the ablation layer which enshrouds the vehicle. Reference 2 has identified the radiation penetration of the ablation layer as the major uncertainty associated with the heat shield design. Furthermore, the coupled flowfield solutions (surface heating and ablation injection rate coupled) reported for the probe forebody have, with one exception,[4] assumed the flow to be laminar. The coupled turbulent solution presented in Ref. 4 was for conditions near the end of the radiative heating pulse. Consequently, both the heating and mass injection rates were small relative to that for maximum heating. Therefore, the question concerning the effect of turbulence on radiative heating with large blowing remains unanswered.

The potential for turbulent flow during Jupiter entry is plausible in view of the fact that a recent experimental study[5] showed that blowing can promote transition on spherically blunted cones for modest blowing rates. Consequently, the objective of this paper is to provide a qualitative description of the potential impact of turbulence on a radiating flowfield with large surface blowing. This is accomplished by calculating the forebody flowfield with coupled carbon-phenolic mass injection for selected freestream entry conditions along an entry trajectory into Jupiter's atmosphere. Both laminar and turbulent flow conditions are assumed. The calculations are made with the turbulent viscous-shock-layer analysis of Ref. 6, and the flow is assumed to be in chemical equilibrium. Particular emphasis is made to identify the potential effect of turbulence on the radiation blockage effectiveness of the injected ablation species.

Analysis

Governing Equations

The equations of motion for reacting gas mixtures in chemical equilibrium are presented by Bird, Stewart, and Lightfoot.[7] The formulation of these equations in body-oriented coordinates appropriate for viscous-shock-layer analysis of laminar flow of radiating and nonradiating gases is presented by Moss,[8,9] whereas the turbulent formulation of the equations is presented by Anderson.[6]

For turbulent flow, the viscous-shock-layer equations are derived using methods analogous to those presented by Dorrance[10] for the turbulent-boundary-layer equations and are expressed in nondimensional form for the coordinate system shown in Fig. 1 as:

$$\frac{\partial}{\partial s}\left[(r+n\cos\theta)^j \rho u\right] + \frac{\partial}{\partial n}\left[(1+n\kappa)(r+n\cos\theta)^j \rho v\right] = 0 \quad (1)$$

s-momentum

$$\rho\left(\frac{u}{1+n\kappa}\frac{\partial u}{\partial s} + v\frac{\partial u}{\partial n} + \frac{uv\kappa}{1+n\kappa}\right) + \frac{1}{1+n\kappa}\frac{\partial p}{\partial s}$$
$$= \sigma^2\left\{\frac{\partial}{\partial n}\left[\mu(1+\epsilon^+)\left(\frac{\partial u}{\partial n} - \frac{u\kappa}{1+n\kappa}\right)\right]\right.$$
$$\left. + \left(\frac{2\kappa}{1+n\kappa} + \frac{j\cos\theta}{r+n\cos\theta}\right)\left[\mu(1+\epsilon^+)\left(\frac{\partial u}{\partial n} - \frac{u\kappa}{1+n\kappa}\right)\right]\right\} \quad (2)$$

n-momentum

$$\rho\left(\frac{u}{1+n\kappa}\frac{\partial v}{\partial s} + v\frac{\partial v}{\partial n} - \frac{u^2\kappa}{1+n\kappa}\right) + \frac{\partial p}{\partial n} = 0 \quad (3a)$$

where the thin shock-layer form of Eq. (3a) is:

$$\frac{\partial p}{\partial n} = \frac{\rho u^2 \kappa}{1+n\kappa} \quad (3b)$$

Energy

$$\rho\left(\frac{u}{1+n\kappa}\frac{\partial H}{\partial s} + v\frac{\partial H}{\partial n}\right) - v\frac{\partial p}{\partial n} + \frac{\rho u^2 v\kappa}{1+n\kappa}$$
$$= \sigma^2\left[\frac{\partial}{\partial n}(\phi_1+\phi_2+\phi_3) + \left(\frac{\kappa}{1+n\kappa} + \frac{j\cos\theta}{r+n\cos\theta}\right)\right.$$
$$\left. \times (\phi_1+\phi_2+\phi_3)\right] - Q \quad (4a)$$

where

$$\phi_1 = \frac{\mu}{N_{Pr}}\left(1+\epsilon^+\frac{N_{Pr}}{N_{Pr,T}}\right)\frac{\partial H}{\partial n} \quad (4b)$$

$$\phi_2 = \frac{\mu}{N_{Pr}}\left[N_{Pr} - 1 + \frac{\epsilon^+ N_{Pr}}{N_{Pr,T}}(N_{Pr,T}-1)\right]u\frac{\partial u}{\partial n}$$
$$- \frac{\mu(1+\epsilon^+)u^2\kappa}{1+n\kappa} \quad (4c)$$

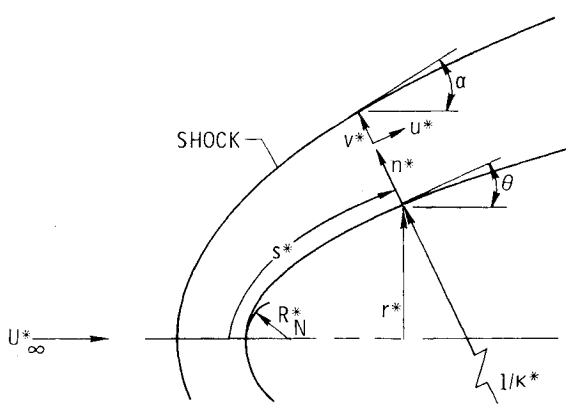

Fig. 1 Coordinate system.

$$\phi_3 = \frac{\mu}{N_{Pr}}\left[N_{Le} - 1 + \epsilon^+ \frac{N_{Pr}}{N_{Pr,T}}(N_{Le,T} - 1)\right]\sum_{i=1}^{N} h_i \frac{\partial C_i}{\partial n} \quad (4d)$$

and

$$H \equiv h + u^2/2 \quad (4e)$$

Elemental continuity

$$\rho\left(\frac{u}{1+n\kappa}\frac{\partial \tilde{C}_l}{\partial s} + v\frac{\partial \tilde{C}_l}{\partial n}\right) = \frac{\sigma^2}{(1+n\kappa)(r+n\cos\theta)^j} \times \frac{\partial}{\partial n}\left\{\left[(1+n\kappa)(r+n\cos\theta)^j \times \frac{\mu}{N_{Pr}}\left(N_{Le} + \epsilon^+ \frac{N_{Pr}}{N_{Pr,T}} N_{Le,T}\right)\frac{\partial \tilde{C}_l}{\partial n}\right]\right\} \quad (5a)$$

where

$$\tilde{C}_l = \sum_{i=1}^{N} \delta_{il} \frac{M_l^*}{M_i^*} C_i \quad (5b)$$

State

$$p = \rho T R^* / \tilde{M}^* C^*_{p,\infty} \quad (6)$$

Boundary Conditions

The boundary conditions at the shock are calculated by using the Rankine-Hugoniot relations. At the wall, the no-slip and no-temperature-jump boundary conditions are used; consequently, $u_w = 0$. The wall temperature and mass injection rate are either specified or calculated. For the calculated mass injection conditions, the ablation process is assumed to be quasisteady and the wall temperature is the sublimation temperature of the ablator surface.

The heat transferred to the wall due to conduction and diffusion is

$$-q_{c,w} = \sigma^2\left(K\frac{\partial T}{\partial n} + \frac{\mu}{N_{Sc}}\sum_{i=1}^{N} h_i \frac{\partial C_i}{\partial n}\right)_w \quad (7)$$

More complete boundary conditions are presented in Ref. 11.

Radiative Transport

The radiative flux q_r is calculated with the radiative transport code RAD.[12,13] The RAD computer code has been incorporated in the present viscous-shock-layer computer code (HYVIS) and streamlined for computational efficiency.

The RAD code accounts for the effects of nongray self-absorption. Molecular band, continuum, and atomic line transitions are included. A detailed frequency dependence of the absorption coefficients is used for integrating over the radiation frequency spectrum and the tangent slab approximation is used for intergrating over physical space. The chemical species considered in the present study for determining the radiative transport are H, H_2, H^+, e^-, C, C_2, C_3, C^+, C^-, CO, O, O_2, O^+, and O^-.

Thermodynamic and Transport Properties

The equilibrium composition is determined by a free-energy minimization calculation as developed in Ref. 14. Thermodynamic properties for specific heat, enthalpy, and free-energy and transport properties for viscosity and thermal conductivity are required for each species considered. Values for the thermodynamic and transport properties are obtained by using polynomial curve fits. The mixture viscosity is obtained by using the semiempirical formula of Wilke.[15]

In this study, the Lewis number and Prandtl number[16] are set equal to 1.1 and 0.64, respectively. Six chemical species are used to describe the hydrogen-helium gas mixture: H, H_2, H^+, e^-, He, and He^+. With carbon-phenolic injection, 19 chemical species are used: the six aforementioned species plus C, C_2, C_3, C^+, C_2H, C_3H, C_4H, C_2H_2, O, O_2, O^+, CO, and CO_2.

Eddy-Viscosity Approximations

A two-layer eddy-viscosity model consisting of an inner law based on Prandtl's mixing-length concept and the Clauser-Klebanoff expression (based on Refs. 17 and 18) for the outer law is used in the present investigation. This model, introduced by Cebeci,[19] assumes that the inner law is applicable for the flow from the wall out to the location where the eddy viscosity given by the inner law is equal to that of the outer law. The outer law is then assumed applicable for the remainder of the viscous layer. It is noted that the eddy viscosity degenerates to approximately zero in the inviscid portion of the shock layer. The degeneracy is expressed in terms of the normal intermittency factor given by Klebanoff.[18]

The turbulent Prandtl and Lewis numbers are assumed to be 0.9 and 1.0, respectively.

Method of Solution

Davis[20] presented a method for solving the viscous-shock-layer equations for stagnation and downstream flow. Moss[8,9] applied this method of solution to reacting multicomponent mixtures. The present method of solution is identical to that of Ref. 8 and, therefore, is not presented.

Results and Discussion

Flowfield results and surface heating rates are presented for the forebody of a probe entering a proposed Jupiter atmosphere. Results are presented with and without ablation injection for both laminar and turbulent flow. The extent to which the radiation from the high-temperature shock layer is blocked by the cooler gases evolved from the carbon-phenolic heat shied is examined. Particular emphasis is focused on the influence of turbulence on radiative heating.

Entry Conditions

In the present study, probe forebodies for both a 50-deg spherically blunted cone and a 43.5-deg (asymptotic half-angle) hyperboloid are considered. Most of the results presented, however, will be for the analytic-shaped hyperboloid because the present viscous-shock-layer analysis experiences difficulties at the sphere-cone tangency point for problems with mass injection. The 43.5-deg hyperboloid was chosen because it has approximately the same drag coefficient ($C_D = 1.25$) as a 50-deg half-angle sphere-cone configuration for equivalent forebody nose and base radii.

The entry trajectory (for either a 50-deg spherically blunted cone or a 43.5-deg hyperboloid) is for an entry into the Jupiter atmosphere where the atmospheric gas model is a revised Ames cool model[3] (78% H_2 + 22% He by volume). The cool atmospheric gas model was used in the present study rather than the nominal (89% H_2 + 11% He) or warm (100% H_2) models, because the cool model provides the most severe entry conditions in terms of both heating rates and heat load. The entry is off the equatorial plane where the trajectory calculation is initiated at an altitude of 1000 km, an inertial entry angle of -9 deg, a relative entry velocity of 48.28 km/s, a latitude of $-6.4°$N, and a heading of 72.5°E. The off-equatorial entry is presently being considered in order to avoid the most intense portion of the ionization belt located near the equatorial plane.

The trajectory was calculated with the POST[21] computer program, maintaining the ballistic coefficient constant at its initial value of 183.9 kg/s. Consequently, the effects of mass loss and shape change are not accounted for in the trajectory calculations. Table 1 presents freestream conditions and stagnation results for no injection. The shock layer thickness

Table 1 Freestream conditions and stagnation results without ablation injection

Time, s	Altitude, km	U_∞^*, km/s	ρ_∞^* kg/m^3	N_{Re_∞}	p_s^*, atm	ρ_s^*/ρ_∞^*	T_s^*,K	n_s^*, cm	q_c^*, MW/m^2	$q_{r,w}^{(-)*}$, MW/m^2
100	157.23	47.98	3.61×10^{-5}	7.40×10^{4}	0.76	12.92	16806	1.65	99	50
102	143.21	47.36	6.88×10^{-5}	1.40×10^{5}	1.40	12.46	17361	1.68	128	117
104	129.53	46.23	1.29×10^{-4}	2.52×10^{5}	2.49	11.99	17747	1.73	152	248
106	116.39	44.27	2.36×10^{-4}	4.38×10^{5}	4.17	11.44	17836	1.80	167	451
107	110.09	42.86	3.17×10^{-4}	5.69×10^{5}	5.24	11.17	17708	1.84	171	562
108	104.05	41.10	4.23×10^{-4}	7.29×10^{5}	6.41	10.85	17438	1.91	170	656
109	98.29	38.97	5.62×10^{-4}	9.20×10^{5}	7.62	10.44	16998	2.00	166	704
110	92.88	36.47	7.39×10^{-4}	1.14×10^{5}	8.74	9.99	16356	2.12	156	677
111	87.86	33.65	9.63×10^{-4}	1.38×10^{6}	9.63	9.43	15471	2.26	140	561
112	83.26	30.59	1.24×10^{-3}	1.64×10^{6}	10.14	8.67	14272	2.44	120	366
113	79.11	27.41	1.56×10^{-3}	1.89×10^{6}	10.23	8.40	12608	2.58	96	150
114	75.42	24.25	1.94×10^{-3}	2.12×10^{6}	9.99	8.66	9929	2.46	68	16
115	72.16	21.24	2.37×10^{-3}	2.32×10^{6}	9.61	11.10	6246	1.98	39	0

and heating rate results are those for the spherically blunted cone which differ slightly from those for the hyperboloid because of the difference in shock curvature in the stagnation region.

Stagnation Point Results

The stagnation point heating rate pulses, both with and without coupled carbon-phenolic mass injection, are presented in Fig. 2. These results demonstrate that the heating is dominated by the radiative heating during the more intense portion of the heating pulse. Furthermore, the coupled carbon-phenolic mass injection reduces the heating substantially. The convective heating is reduced to essentially zero during most of the radiative heating pulse and the radiative heating is reduced substantially. For example, at the time of peak radiative heating, the radiative heating rate with coupled mass injection is only 37% of the value for no mass injection.

Probe Forebody Solutions

To investigate the extent of radiative blockage along the probe forebody, flowfield calculations are made for three trajectory times corresponding to peak radiative heating (109 s), heating rates typical of peak heating for entry into a nominal atmosphere (111 s), and a more modest heating environment near the end of the radiative heating pulse (113 s). Reference 11 presents results for each of the three trajectory times; this paper, however, will concentrate on the results for the 111-s case. The solutions with coupled carbon-phenolic mass injection are for a 43.5-deg hyperboloid configuration.

Effect of Injection and Turbulence on Distribution Quantities

Figures 3-4 present results that show the effect of both coupled carbon-phenolic mass injection and turbulence on radiative heating (Fig. 3) and convective heating (Fig. 4) distributions for a trajectory time of 111 s. The coupled carbon-phenolic mass injection distributions are shown in Fig. 5. The impact of the coupled injection on radiative heating is very pronounced in that, generally, the radiative heating is reduced substantially. When the flow is assumed to be laminar, the radiation blockage results obtained in this study are similar to those obtained in Ref. 4, even though the peak heating rate is much greater (the radiative heating is 63% greater) than that considered in Ref. 4. Three areas of similarity are noted. First, the larger the no-injection stagnation point heating rate, the larger the radiation blockage for coupled carbon-phenolic injection (the blockage is 0.63, 0.61, and 0.4 for trajectory times of 109, 111, and 113 s, respectively). Second, the radiation blockage down-

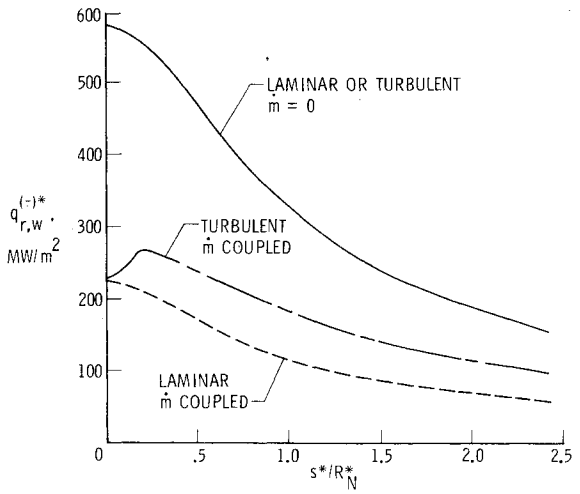

Fig. 3 Effect of coupled carbon-phenolic injection and turbulence on radiative heating for a 43.5-deg hyperboloid (time = 111 s).

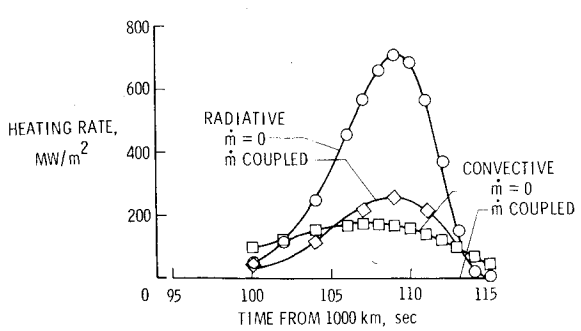

Fig. 2 Effect of coupled carbon-phenolic mass injection on stagnation point heating.

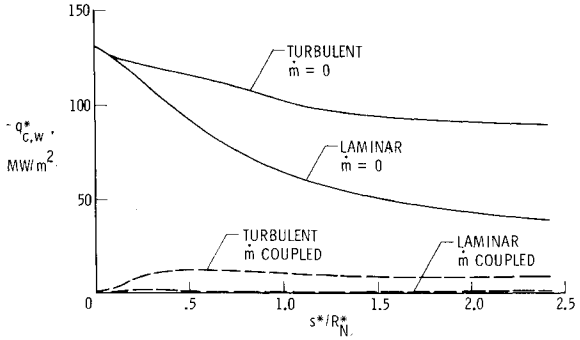

Fig. 4 Effect of coupled carbon-phenolic injection and turbulence on convective heating for a 43.5-deg hyperboloid (time = 111 s).

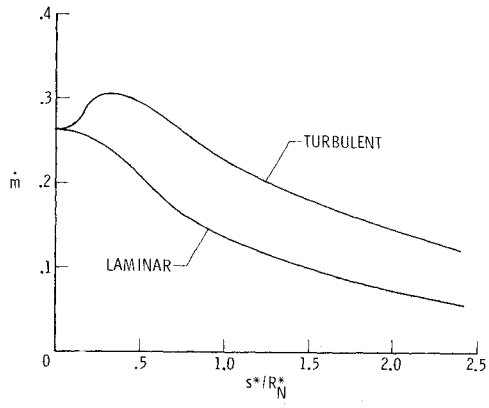

Fig. 5 Comparison of coupled carbon-phenolic mass injection distributions for laminar and turbulent flow (time = 111 s).

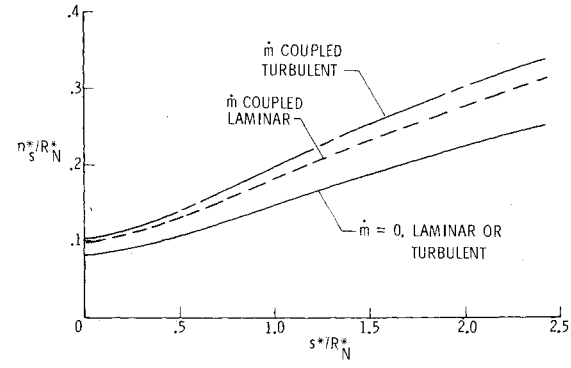

Fig. 6 Effect of coupled carbon-phenolic mass injection and turbulence on shock-layer thickness distributions (time = 111 s).

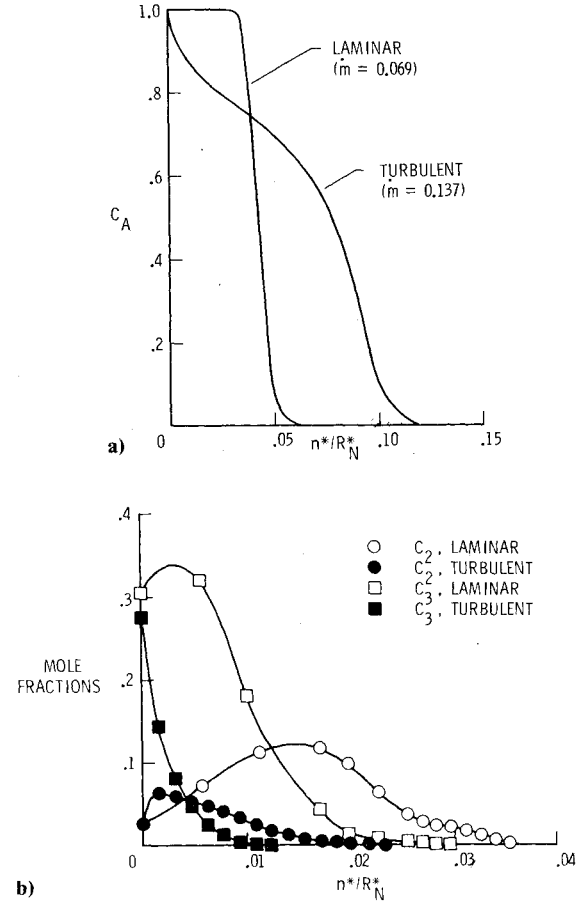

Fig. 7 Effect of turbulence on concentration distributions (time = 111 s, $s^*/R_N^* = 2.1$): a) ablation mass fractions, b) concentration of major radiation absorbers.

stream of the stagnation point is, in general, slightly greater than the corresponding stagnation point value. For example, the radiation blockage for the 111-s case is 0.61 at the stagnation point, whereas it is 0.64 at the end of the probe forebody. However, for more moderate radiative heating conditions (time = 113 s), the radiative blockage downstream of the stagnation region decreases rather than increases, and, in fact, the injection causes an augmentation in the radiative heating.[11] The augmented radiative heating is the third area of agreement with previous calculations.[4] For the turbulent solutions, the flow is assumed to undergo instantaneous transition at s^*/R_N^* equal to 0.1. The no-injection radiative heating rates calculated for turbulent flow are essentially the same as the corresponding laminar results. The reason that turbulence has an insignificant effect on the no-injection radiative heating values is that the absorption of radiation within the boundary layer for hydrogen-helium gas mixtures is small,[22] and most of the radiation incident at the wall originates external to the boundary layer. This is demonstrated in Ref. 22 where the radiative heating predicted for Jupiter entry conditions using an inviscid analysis agrees very well with the values obtained using the present VSL analysis.

For the coupled flowfield solutions with large ablation injection, there exists a relatively cool layer of gas adjacent to the surface that strongly absorbs the radiation that originates in the high-temperature portion of the shock layer. In contrast with the no-injection solution, turbulence has a significant effect on the radiative heating for the solutions with coupled carbon-phenolic injection. Figure 3 presents a comparison of coupled radiative heating distributions for both laminar and turbulent flow. For turbulent flow, the radiative heating rates are greater than the corresponding laminar results. Therefore, turbulence effects a significant reduction in the radiation blockage. This is particularly true since not only is the turbulent radiative heating greater than the corresponding laminar results, but also, the coupled mass injection rate is much greater (Fig. 5) for the turbulent solutions.

During most of the radiative heating pulse, the coupled carbon-phenolic mass injection rate is so large (Fig. 5) that the convective heating becomes very small or insignificant (Fig. 4) when compared with the coupled radiative heating values. Figure 4 presents a comparison of the convective heating rates both laminar and turbulent with and without injection. For a trajectory time of 111 s, the coupled convective laminar heating is insignificant and the coupled convective turbulent heating never exceeds 10% of its no-injection value. As the end of the radiative heating pulse is approached, the injection is not so massive and the convective heating becomes significant, particularly if the flow is turbulent. Even so, the calculated results show that the probe forebody convective heating is very small relative to the radiative heating, even if turbulent, during most of the radiative heating pulse.

Since the coupled ablation injection rates are so massive near peak heating, the structure of the shock layer is necessarily altered. Figure 6 presents a comparison of the shock-layer thickness distribution both with and without injection. The shock-layer thickness with coupled injection is significantly greater than the corresponding no-injection values.

Effect of Injection and Turbulence on Profile Quantities

In this section, attention is focused on why the present turbulence model has such an adverse effect on radiation blockage. This is accomplished by comparing many of the flowfield profile quantities (Figs. 7-9) both with and without turbulence. These comparisons are made for a body location near the aft end of the probe ($s^*/R_N^* = 2.1$). At this body location, the radiation blockage for the laminar solution is 0.65, whereas for turbulent flow, the blockage is only 0.39, a

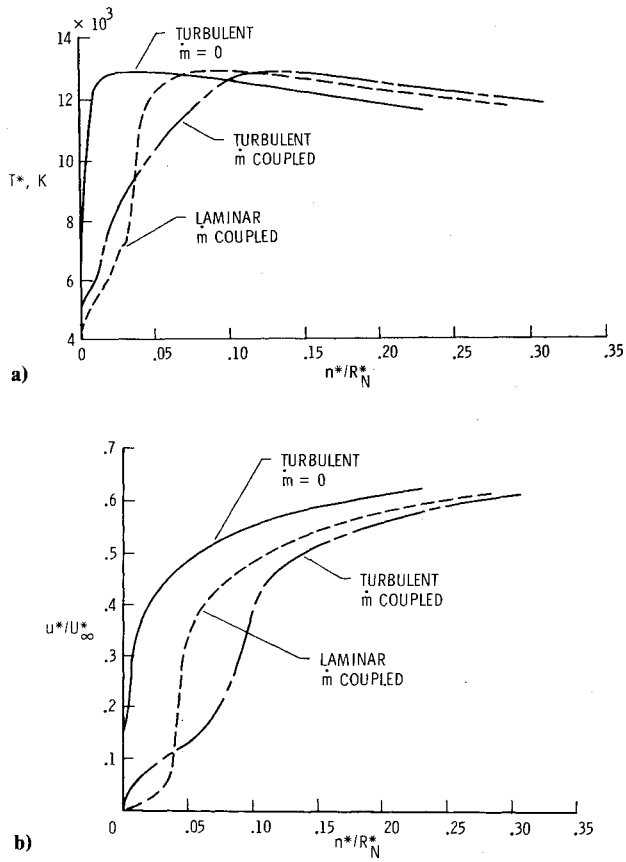

Fig. 8 Effect of coupled carbon-phenolic injection and turbulence on profile quantities (time = 111 s, $s^*/R_N^* = 2.1$): a) temperature profiles, b) tangential velocity profiles.

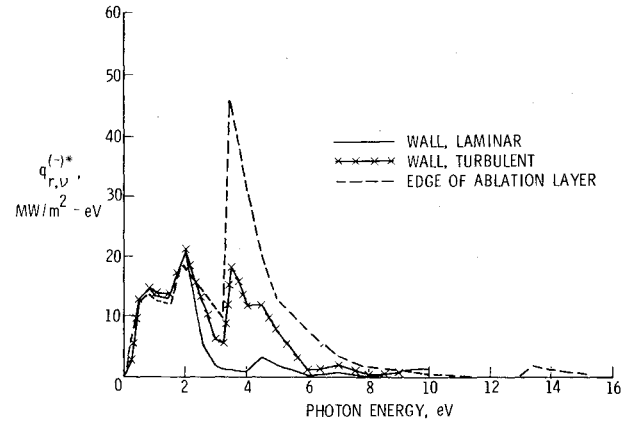

Fig. 9 Effect of carbon-phenolic injection and turbulence on blocking the continuum spectral flux to the wall (time = 111 s, $s^*/R_N^* = 2.1$).

40% reduction in radiation blockage with a 98% increase in coupled carbon-phenolic mass injection.

The reason that turbulence has such an adverse effect on radiative heating with ablation injection is that turbulence significantly alters the extent and composition of the ablation layer. Figure 7 demonstrates the dramatic effect of turbulence on both the ablation layer thickness (Fig. 7a) and the chemical composition within the ablation layer (Fig. 7b). The effect of turbulence on the temperature and tangential velocity profiles are demonstrated in Figs. 8a and 8b, respectively. The combination of a larger coupled injection rate and enhanced diffusion for the turbulent solution results in a much thicker ablation layer (the distance from the wall for which ablation products are present). Near the surface, however, the concentration of ablation products is less for the turbulent solution because of the enhanced diffusion. Of more significance is the fact that turbulence brings the high-temperature shock-layer gases closer to the surface, thereby causing the highly absorbing molecules to dissociate. Reference 4 shows that most of the radiation blockage for Jupiter entry conditions is due to the absorption by the C_2 and C_3 molecules. The thinning of the molecular species near the surface is clearly depicted in Fig. 7b which shows a comparison of the laminar and turbulent species concentration profiles for both the C_2 and C_3 molecules. The C_2 and C_3 concentrations for the turbulent solution are, in general, substantially less than those for the laminar solution. Furthermore, these species do not extend as great a distance away from the wall as for the laminar case. Consequently, the optical thickness of the ablation layer is much thinner than that for the laminar solution.

The reduced absorption within the ablation layer due to turbulence is clearly evident in Fig. 9 which presents the continuum (see Ref. 11 for effect on line radiation) spectral flux incident at the edge of the ablation layer and that incident at the wall for both laminar and turbulent flow. The spectral region where the largest differences exist between the laminar and turbulent results is between 2 and 6 eV; the spectral region[1] where C_2 and C_3 contributes to the radiation absorption.

Turbulence Model Considerations

The foregoing results demonstrate that turbulence can have an adverse influence upon the effectiveness of carbon-phenolic ablation products in blocking radiation. (See Ref. 11 for results that demonstrate the sensitivity of the radiative heating to variations in turbulent model parameters and flow conditions.) However, the surface mass transfer rates considered in this report exceed the available data base by a factor of 10 to 100 which makes the use of currently available turbulence models questionable at best. The two-layer model proposed by Cebeci[19] has been selected on the basis that it has been applied with success by Cebeci and a number of other investigators to most of the available experimental data. In an unpublished investigation, the present authors have applied the Cebeci turbulence model to analyze some of the experimental data presented by Feldhuhn[5] using both a viscous-shock-layer and a boundary-layer computer code. The results of these two analyses showed excellent agreement with Feldhuhn's data, except at the turbulent stagnation point. A number of other mixing length turbulence models as well as a two-equation turbulence model[23] have been considered for application in the present viscous-shock-layer computer code. Since all turbulence models depend upon experimental data to define empirical functions and/or constants, it is unlikely that the selection of any other available turbulence model would improve the confidence in the present results. Therefore, the present results should be viewed in the context that turbulence may substantially reduce the effectiveness of carbon-phenolic ablation products as a radiation heat shield.

Concluding Remarks

Heating and flowfield results are presented for the forebody of a 43.5 deg hyperboloid entering the atmosphere of Jupiter. The turbulent solutions with coupled carbon-phenolic mass injection are the first to be reported in the literature for the present problem—large mass injection and a flowfield environment that is dominated by radiation transfer. Therefore, the present study is significant in that first, it demonstrates that a solution capability exists for such problems and, second, it is the first analysis to show that turbulence can significantly increase the surface radiative heating rate with coupled ablation injection. For the no-blowing solutions, turbulence is shown to have no impact on the surface radiative heating. However, with ablation in-

jection, the eddy viscosity alters the composition within the ablation layer, such that the effectiveness of the relatively cool ablation layer to absorb or block the radiation that originates in the high-temperature region of the shock layer is greatly reduced. Consequently, this study should promote interest in research which considers the impact of turbulence on the radiative heating for outer planet entry conditions and which considers an experimental program to evaluate and develop turbulence modeling techniques appropriate for massively blown shock layers.

References

[1] Moss, J.N., Jones, J.J., and Simmonds, A.L., "Radiative Flux Penetration Through a Blown Shock Layer for Jupiter Entry Conditions," AIAA Paper 78-908, 2nd AIAA/ASME Thermophysics and Heat Transfer Conference, Palo Alto, Calif., May 1978.

[2] Nelson, H.F. and Mezines, S.A., "Parametric Analysis of Jupiter Probe Heat Shield Recession Uncertainties," AIAA Paper 78-919, 2nd AIAA/ASME Thermophysics and Heat Transfer Conference, Palo Alto, Calif., May 1978.

[3] Sutton, K., Jones, J.J., and Powell, R.W., "Effects of Atmospheric Structure on Radiative Heating for Jupiter Entry Probe," AIAA Paper 78-185, AIAA 16th Aerospace Sciences Meeting, Huntsville, Ala., Jan. 1978.

[4] Moss, J.N., Anderson, E.C., and Bolz, C.W., "Aerothermal Environment for Jupiter Entry Probes," AIAA Paper 76-469, AIAA 11th Thermophysics Conference, San Diego, Calif., June 1976; also, *Progress in Astronautics and Aeronautics—Thermophysics of Spacecraft and Outer Planet Entry Probes,* Vol. 56, edited by A.M. Smith, AIAA, New York, 1977, pp. 333-354.

[5] Feldhuhn, R.H., "Heat Transfer From a Turbulent Boundary Layer on a Porous Hemisphere," AIAA Paper 76-119, AIAA 14th Aerospace Sciences Meeting, Washington, D.C., Jan. 1976.

[6] Anderson, E.C., Moss, J.N., and Sutton, K., "Turbulent Viscous-Shock-Layer Solutions With Strong Vorticity Interaction," AIAA Paper 76-120, AIAA 14th Aerospace Sciences Meeting, Washington, D.C., Jan. 1976; also *Journal of Spacecraft and Rockets,* Vol. 14, Jan. 1977, pp. 32-37.

[7] Bird, R.B., Stewart, W.E., and Lightfoot, E.N., *Transport Phenomena,* John Wiley & Sons, Inc., New York, 1960.

[8] Moss, J.N., "Reacting Viscous-Shock-Layer Solutions With Multicomponent Diffusion and Mass Injection," NASA TR-411, 1974.

[9] Moss, J.N., "Stagnation and Downstream Viscous-Shock-Layer Solutions With Radiation and Coupled Ablation Injection," AIAA Paper 74-73, AIAA 12th Aerospace Sciences Meeting, Washington, D.C., Jan. 1974; also *AIAA Journal,* Vol. 14, Sept. 1976, pp. 1311-1317.

[10] Dorrance, W.H., *Viscous Hypersonic Flow,* McGraw-Hill Book Co., Inc., 1962.

[11] Moss, J.N., Anderson, E.C., and Simmonds, A.L., "The Impact of Turbulence on a Radiating Shock Layer With Coupled Ablation Injection," AIAA Paper 78-1186, AIAA 11th Fluid and Plasma Dynamics Conference, Seattle, Wash., July 1978.

[12] Nicolet, W.E., "Advanced Methods for Calculating Radiation Transport in Ablation-Product Contaminated Boundary Layers," NASA CR-1656, 1970.

[13] Nicolet, W.E., "User's Manual for the Generalized Radiation Transfer Code (RAD/EQUIL)," NASA CR-116353, 1969.

[14] Stroud, C.W. and Brinkley, K.L., "Chemical Equilibrium of Ablation Materials Including Condensed Species," NASA TN D-5391, 1969.

[15] Wilke, C.R., "A Viscosity Equation for Gas Mixtures," *Journal of Chemical Physics,* Vol. 18, April 1950, pp. 517-519.

[16] Grier, N.T., "Calculation of Transport Properties and Heat-Transfer Parameters of Dissociating Hydrogen," NASA TN D-1406, 1962.

[17] Clauser, F.H., *The Turbulent Boundary Layer,* Vol. IV of *Advances in Applied Mathematics,* edited by H.L. Dryden and Th. Von Kármán, Academic Press, Inc., 1956, pp. 1-51.

[18] Klebanoff, P.S., "Characteristics of Turbulence in a Boundary Layer With Zero Pressure Gradient," NACA Rept. 1247 (supersedes NACA TN 3178), 1955.

[19] Cebeci, T., "Behavior of Turbulent Flow Near a Porous Wall With Pressure Gradient," *AIAA Journal,* Vol. 8, Dec. 1970, pp. 2152-2156.

[20] Davis, R.T., "Numerical Solution of the Hypersonic Viscous Shock-Layer Equations," *AIAA Journal,* Vol. 8, May 1970, pp. 843-851.

[21] Brauer, G.L., Cornick, D.E., and Stevenson, R., "Capabilities and Applications of the Program to Optimize Simulated Trajectories (POST)," NASA CR-2770, 1977.

[22] Zoby, E.V., Sutton, K., Olstad, W.B., and Moss, J.N., "An Approximate Inviscid Radiating Flow-Field Analysis for Outer Planet Entry Probes," AIAA Paper 78-189, AIAA 16th Aerospace Sciences Meeting, Huntsville, Ala., Jan. 1978.

[23] Anderson, E.C. and Wilcox, D.C., "Transitional Boundary-Layer Solutions Using a Mixing-Length and a Two-Equation Turbulence Model," NASA CR-2986, 1978.